JOURNAL OF THERMOPHYSICS AND HEAT TRANSFER
Vol. 11, No. 3, July–September 1997

Line-of-Sight Temperature and Species Profiles Determined from Spectral Transmittances

C. F. Mallery* and S. T. Thynell†
Pennsylvania State University, University Park, Pennsylvania 16802

Line-of-sight (LOS) variations of temperature and concentrations of CO and H_2O within a simulated high-pressure flame are deduced using an inverse analysis. In this work, synthetic spectral transmittances, acquired by a Fourier transform infrared spectrometer along a single LOS, represent the experimental data. The theoretical basis of the analysis is that spectral variations in the absorption coefficient contain information about spatial variations in temperature and species concentrations. The Marquardt–Levenberg method is used to solve for the temperature and species concentrations. Accurate spatial variations of temperature and species concentrations can be recovered when changes in the spectral transmittances caused by noise are smaller than those changes caused by spatial variations in temperature and species concentrations. The recovered centerline temperatures and species concentrations are, respectively, within 5 and 20% of the synthetic values, when the variations in spectral transmittance caused by noise are about the same as that caused by spatial variations in temperature and species concentrations. As temperature increases, a redistribution in the molecular states decreases the spectral absorptances, thereby causing the analysis to become more sensitive to the effects of noise.

Nomenclature

c = speed of light, m/s
E' = rotational energy of lower state
F = spectral transmittance
g = normalized rovibrational (rotational–vibrational) line shape function
h = Planck's constant
k = Boltzmann's constant
L = 0.0025 m, half of path length
m_P = order of power series used to approximate partial-pressure profiles
m_T = order of power series used to approximate temperature profiles
N = number of molecules per cm^3 per atm
N_d = number of data points in measurement
N_{np} = number of gaseous species present along the line of sight that is not being quantified
N_p = number of half-periods used to calculate integral over the wave number range
N_r = number of rovibrational transitions
N_s = number of species
N_x = order of quadrature used in the integral along path length
N_ν = order of quadrature used in convolution integral
P = pressure, atm
$P_{i,m}$ = coefficients for partial pressure of ith species
Q = partition function
S = line intensity
T = temperature, K
T_m = coefficients for temperature profile
w_l = weights for Gauss–Legendre quadrature
$\boldsymbol{X}_n(x)$ = row vector of species mole fractions, $\boldsymbol{X}_n = (X_{N_2}, X_{CO}, X_{H_2O})$
x = distance along the line of sight from the center of the flame
z = x/L
α = absorption coefficient
γ_p = half-width at half-height of spectral line, cm^{-1}
Δ_{max} = maximum retardation of moving mirror, cm
$\Delta\nu_n$ = half-period of instrument line shape, cm^{-1}
ν = wave number, cm^{-1}
σ = standard deviation
Φ = temperature exponent for γ_p
χ^2 = sum of squares, Eq. (11)
ω = Gaussian distribution function

Subscripts
i = ith species
j = jth rovibrational transition
k, l = index for quadrature
noise = quantity affected by noise
r = reference state
t = total
true = true quantity
0 = rovibrational line center

Superscripts
1, 2 = steps 1 and 2 of data-reduction routine
^ = modeled quantity
~ = synthetic quantity

Introduction

THERE is a strong current interest to continue developing nonintrusive diagnostic techniques for deducing temperature and species concentrations within combustion systems.[1] Information on temperature and species concentrations from such measurements is needed to advance our understanding of the physical and chemical processes that occur during combustion.[1] This understanding, in turn, can be used by synthesizers for the design of propellants that produce fewer harmful pollutants, by physical chemists for the validation of detailed chemical kinetic reaction mechanisms, and by engineers for the formulation of complex models of physicochemical processes that occur in rocket motors and gun systems.

Received Oct. 24, 1996; presented as Paper 97-0120 at the AIAA 35th Aerospace Sciences Meeting, Reno, NV, Jan. 6–9, 1997; revision received Jan. 24, 1997; accepted for publication Jan. 25, 1997.

*Graduate Research Assistant and URI Fellow, Department of Mechanical Engineering.

†Associate Professor, Department of Mechanical Engineering. Member AIAA.

High-pressure strand burners[2–4] and low-pressure flat-flame burners[5–7] with optical access for nonintrusive diagnostics have been employed to study the combustion behavior of solid propellants and premixed gases, respectively. The use of nonintrusive diagnostic techniques within these burner configurations has allowed a determination of temperature and chemical composition within the flame zone. Many measurements using strand burners,[1–4] flat-flame burners,[5–7] and laminar diffusion flames[8] have been reported using line of sight (LOS) techniques, such as uv/visible,[1,2] multichannel mid-infrared (mid-IR),[3] and Fourier transform infrared (FTIR) absorption spectroscopy.[4–6] Although temperature and species concentrations can vary along the LOS within the flame, it appears that many investigators have not accounted for this effect in their data-reduction analysis.[1–6] In essence, their results represent a weighted average of temperature and species concentrations over the measurement's path length. The development of point-based nonintrusive diagnostic techniques, such as laser-induced fluorescence (LIF) and planar LIF (PLIF),[1] has been highly successful; however, their applications in high-pressure flames of solid propellants cause some concern with treatment of quenching effects.

In past research with LOS instruments, investigators employed multiple paths through the flame for radial temperature and species concentration profiling along with Abel's inversion technique.[9] Diffusion[7] and premixed[8] flames are well suited to inversion techniques because the flames are stable and fixed in space to allow probing at different radial positions. However, the use of multiple paths in flames of solid propellants is quite challenging in view of the required high pressures (which optically limit the flame width), relatively high burning rates, and a moving burning surface (short measurement times, generally 30 s or less).

Recent efforts focused on one-dimensional ignition and steady deflagration models of solid propellants[10,11] with detailed finite rate chemical kinetics[12,13] have significantly increased the demand for accurate data on the variation of temperature and species concentration in the direction of flow of products. Experimental data acquired at and along the centerline within the flame should be particularly useful in validating these complex models. It is evident that mathematical methods that attempt to provide an insight into the variations of temperature and species concentration along the LOS should be pursued. In this work, a detailed analysis is provided on the application of the spectral transmittance for the determination of temperature and species profiles of IR-active gases using a single LOS spectrum.

Theory and Data Reduction

Let us consider that the modulated beam of an FTIR spectrometer propagates through a solid-propellant flame as depicted in Fig. 1. The size of the modulated beam is much smaller than the width of the flame. Within the modulated beam, vertical variations of temperature and species concentration are assumed to be negligible. The beam travels across the center of the propellant strand, perpendicular to the direction of flow of hot gases, and the transmitted component is detected by the spectrometer. In developing a model of the spectral transmittance, the interaction of the modulated beam with hot gases, along with effects arising from the instrument itself, must be considered. The modeled spectral transmittance is compared with the measured spectral transmittance to recover spatial profiles of temperature and concentrations of IR-active species. A large number of spectral data points is utilized, and, in this work, all of the measured spectral transmittances are generated synthetically.

Model of Spectral Transmittance

In modeling the spectral transmittance acquired by an FTIR spectrometer operating at a low spectral resolution, the instrumental effects must be considered to correctly deduce temperature and species concentrations.[14] By assuming that spectral lines cannot be resolved because of the finite resolution of the spectrometer, a convolution of the true transmittance with the instrument line shape (ILS) should reproduce the synthetic (measured) spectral transmittance $F(\nu)$. Such a convolution may be expressed by

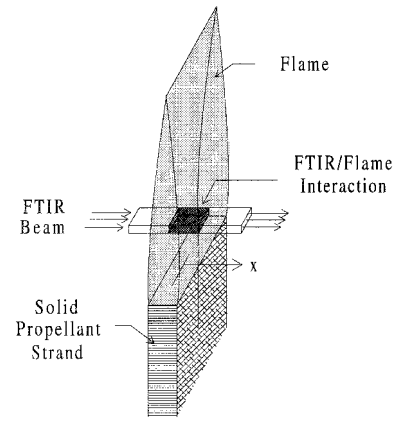

Fig. 1 Schematic diagram of the FTIR beam propagation through the solid-propellant flame.

$$F(\nu) = \int_{-\infty}^{\infty} F_{\text{true}}(\nu') f(\nu - \nu')\, \mathrm{d}\nu' \tag{1}$$

where the symbols are defined in the Nomenclature. For triangular apodization, the ILS is[14]

$$f(\nu - \nu') = \frac{\Delta_{\max} \sin^2[\pi\Delta_{\max}(\nu - \nu')]}{[\pi\Delta_{\max}(\nu - \nu')]^2} \tag{2}$$

For molecular gases, such as those that appear in most solid-propellant flames, scattering is negligible compared to absorption. If small absorbing particles are present, such as soot, they possess broadband absorption characteristics and can be accounted for in the analysis. The true spectral transmittance can therefore be written as[8]

$$F_{\text{true}}(\nu) = \exp\left\{-2 \int_0^L \sum_{i=1}^{N_s} \sum_{j=1}^{N_r} \boldsymbol{\alpha}_{i,j}[\nu, T(x), X_n(x)] P_i(x)\, \mathrm{d}x\right\} \tag{3}$$

where the absorption coefficient and the line intensity are, respectively, given by[15]

$$\alpha_{i,j}(\nu, T, X_n) = S_{i,j}(T) g(\nu - \nu_{0,i,j}, T, X_n) N \tag{4}$$

$$S_{i,j}(T) = S(T_r) \frac{Q(T_r)}{Q(T)} \frac{1 - \exp(-hc\nu_{0,i,j}/kT)}{1 - \exp(-hc\nu_{0,i,j}/kT_r)} \times \exp\left(\frac{E'}{k} \times \frac{T - T_r}{TT_r}\right) \tag{5}$$

Values of the partition function are determined from curve fits provided in the HITRAN database.[16] The two terms involving $\exp(-hc\nu_{0,i,j}/kT)$ correct for induced emission, whereas the other exponential term accounts for the Boltzmann distribution of molecular states with temperature. In FTIR transmission spectroscopy, spontaneous emission does not directly contribute to the measured signal,[14] and therefore, is not included in the line intensity. The normalized line shape in Eq. (4) depends on the state of the absorbing gases. In the mid-IR (500–5000 cm^{-1}) at the pressures considered in this work (10 atm), pressure broadening is dominant. Therefore, a Lorentzian line shape given by

$$g(\nu - \nu_{0,i,j}, T, X_n) = \frac{\gamma_{p_{i,j}}(T, X_n)/\pi}{(\nu - \nu_{0,i,j})^2 + \gamma^2_{p_{i,j}}(T, X_n)} \tag{6}$$

is used. The dependence of the line's half-width at half-height (HWHH) on temperature, pressure, and species mole fractions is expressed as[17]

$$\gamma_{p_{i,j}} = \sum_{n=1}^{N_s+N_{\text{np}}} \gamma_{p_{r,i,j}}^{i-n} \left(\frac{T_r}{T}\right)^{\Phi_{i,j}^{i-n}} \frac{P_t}{P_r} X_n \tag{7}$$

Here, the reference pressure and temperature are, respectively, 1 atm and 296 K. Data on broadening parameters for $CO-N_2$ and $CO-H_2O$ were obtained from Ref. 17, whereas the self-broadening reference HWHH was taken from Ref. 18. In this work, CO and N_2 were assumed to have the same CO temperature exponent, since variations in the CO self-broadening temperature exponent with rotational index were not found in the literature. Values of the reference HWHH and temperature coefficients for H_2O were obtained from Ref. 19. CO and N_2 were assumed to have the same collisional broadening effect on H_2O in this work, since no collisional broadening parameters for H_2O-CO were found in the literature. This analysis assumes that the collisional broadening parameters of all molecules are independent of vibrational states,[17] and therefore, have only a rotational dependence. Discussion of the reference HWHH and temperature coefficients, which are functions of the rotational index number,[18,20] are available.[17,19] Nitrogen is the only IR-inactive gas considered, and its mole fraction is evaluated from

$$X_{N_2} = 1 - X_{H_2O} - X_{CO} \tag{8}$$

Integrals in Eqs. (1) and (3) are evaluated numerically. Integration over the path length is performed using a 16-point Gauss–Legendre quadrature.[21] The convolution integral is more involved because of the oscillatory nature of the ILS coupled with an infinite limit of integration. The integral is divided into half-periods, and a 16-point Gauss–Legendre quadrature is applied to approximate the integral over each half-period. The spectral transmittance is computed from

$$F(\nu) = \sum_{n'=-N_p}^{N_p} \frac{\Delta\nu_{n'}}{2} \sum_{l=1}^{N_\nu} \prod_i \prod_j \times \exp\left\{-L \sum_{k=1}^{N_s} \alpha_{i,j}[\nu_{l,n'}, T(x_k), X_n(x_k)] P_i(x_k) w_k\right\} \times f(\nu - \nu_{l,n'}) w_l \tag{9}$$

The use of Eq. (9) in an inverse model allows a determination of the temperature and partial-pressure profiles from spectral transmittance data. In this work, the temperature and partial pressures are assumed to vary according to power series containing only even-ordered terms as a result of flame symmetry. The functional forms of both the synthetic (representing measured data) and modeled temperature and partial-pressure profiles are, respectively, given by

$$T(z) = T_0 + T_1 z^2 + \cdots + T_{m_T} z^{2m_T} \tag{10a}$$

$$P_i(z) = P_{i,0} + P_{i,1} z^2 + \cdots + P_{i,m_P} z^{2m_P} \tag{10b}$$

The maximum temperature is located at the midpoint along the beam in Fig. 1 because the propellant burns in a cool, inert atmosphere. The partial-pressure profiles of CO and H_2O are more than likely monotonically decreasing functions from the center to the edge of the flame. In this work, the general features of the inverse technique are explored, and it is desirable to keep these profiles simple.

Solution Methodology

The spectral absorption coefficient depends on temperature and partial pressures of IR-active species through the line intensity, line shape, and the path-length integral in Eq. (3). This spectral dependence allows temperature and species profiles to be deduced from the spectral variation in the synthetic transmittance. The inverse problem seeks to minimize the quantity

$$\chi^2 = \sum_{n=1}^{N_d} [\tilde{F}_n - \hat{F}_n(\hat{T}_0, \hat{T}_1, \ldots, \hat{T}_{\hat{m}_T}, \hat{P}_{i,0}, \hat{P}_{i,1}, \ldots, \hat{P}_{i,\hat{m}_P})]^2 \tag{11}$$

The Marquardt–Levenberg method,[21] which is a nonlinear least-squares inverse technique, is used to iteratively determine the coefficients for the temperature ($\hat{T}_0, \hat{T}_1, \ldots, \hat{T}_{\hat{m}_T}$) and partial pressures ($\hat{P}_{i,0}, \hat{P}_{i,1}, \ldots, \hat{P}_{i,\hat{m}_P}$) from synthetic spectral transmittances. The synthetic transmittances are computed using the model previously described and using a synthetic set of coefficients ($\tilde{T}_0, \tilde{T}_1, \ldots, \tilde{T}_{\tilde{m}_T}$) for the temperature and ($\tilde{P}_{i,0}, \tilde{P}_{i,1}, \ldots, \tilde{P}_{i,\tilde{m}_P}$) for the partial pressures of CO and H_2O. The Marquardt–Levenberg method is well documented[21–23] and therefore not presented in this paper. Derivatives required within the inverse algorithm are evaluated using a forward finite difference technique. In addition, convergence of the iterative procedure is established when the change in the χ^2 from one iteration to the next is $<10^{-4}$.

Implementation of the inverse method with the previously described theoretical model results in an algorithm that is quite time-consuming on the computer because of the oscillatory nature of the ILS. The algorithm is implemented in two steps.

Step 1: LOS-average temperature, $\hat{T}_0^1$, and partial pressures of CO and H_2O, $\hat{P}_{CO,0}^1$ and $\hat{P}_{H_2O,0}^1$, are determined.

Step 2: The coefficients, $\hat{T}_0^2, \hat{T}_1^2, \ldots, \hat{T}_{\hat{m}_T}^2, \hat{P}_{CO,0}^2, \hat{P}_{CO,1}^2, \ldots, \hat{P}_{CO,\hat{m}_P}^2$, and $\hat{P}_{H_2O,0}^2, \hat{P}_{H_2O,1}^2, \ldots, \hat{P}_{H_2O,\hat{m}_P}^2$, are evaluated using $\hat{T}_0^1$, $\hat{P}_{CO,0}^1$, and $\hat{P}_{H_2O,0}^1$ as initial guesses.

Discussion of Results

To illustrate the application of the inverse analysis, synthetic spectra from a simulated flame of a nitramine-based propellant are used. It is well known that many nitramine-composite propellants produce a dark zone whose length varies (up to 1 cm) with pressure.[24] The dark-zone region contains a wide variety of IR-active species, including, among others, NO, CO, CO_2, H_2O, N_2O, HCN, and many different hydrocarbon species formed from binder decomposition and secondary reactions. The considered species are, to a large extent, formed in the primary reaction zone near the burning surface. Two of these species are considered in this analysis: CO and H_2O. Their high-temperature absorption characteristics are well known. A total pressure of 10 atm, partial pressures of 2.5 atm for CO and H_2O, a dark-zone temperature of 1300 K, and a path length of 0.005 m are considered. These conditions lead to synthetic spectral transmittances that are consistent with measurements through an actual flame.[2,3]

It is assumed that the FTIR spectrometer operates at a spectral resolution of 1.93 cm^{-1}. For a rapid-scanning spectrometer, such as the Nicolet 740, spectra can be acquired at the rate of 5 Hz at this spectral resolution. Coefficients for temperature and partial-pressure profiles are recovered using 415 synthetically generated transmittances covering two spectral ranges: 1900–2100 and 3750–3950 cm^{-1}. The first spectral range covers the P branch of the ν_0 band of CO, and uses 1000 rovibrational transitions; the second spectral range covers the ν_1 and ν_3 bands of H_2O and uses 6000 rovibrational transitions. The discussion of results is first focused on the accuracy of the numerical evaluation of Eq. (9), then on the recovery of temperature and species concentration profiles from noise-free spectra, and is concluded by the effects of noise.

Numerical Evaluation of $F(\nu)$

It is well known that the accuracy with which the direct problem is evaluated has a strong impact on the recovered quantities of interest in inverse problems.[25] Therefore, an as-

Table 1 Effect of number of periods and quadrature orders on the accuracy of the numerical evaluation of the spectral transmittance, $F(\nu)$

		$F(\nu)$ of CO at $\nu = 2073.1$ cm^{-1} $P_{CO} = 2.5 - 1.25z^2$			$F(\nu)$ of H_2O at $\nu = 3854.1$ cm^{-1} $P_{H_2O} = 2.5 - 1.25z^2$		
N_p	N_ν	$N_x = 4$	8	40	$N_x = 4$	8	40
10	4	0.6097810	0.6098278	0.6098277	0.7662037	0.7661680	0.7661678
	8	0.6098490	0.6098958	0.6098957	0.7661993	0.7661637	0.7661635
	16	0.6098488	0.6098956	0.6098955	0.7661993	0.7661637	0.7661635
	40	0.6098488	0.6098956	0.6098955	0.7661993	0.7661637	0.7661635
30	4	0.6071501	0.6071971	0.6071970	0.7650127	0.7649762	0.7649765
	8	0.6072169	0.6072640	0.6072639	0.7650084	0.7649725	0.7649723
	16	0.6072167	0.6072638	0.6072637	0.7650084	0.7649725	0.7649723
	40	0.6072167	0.6072638	0.6072637	0.7650084	0.7649725	0.7649723
50	4	0.6066033	0.6066502	0.6066501	0.7647816	0.7647455	0.7647454
	8	0.6066705	0.6067175	0.6067174	0.7647773	0.7647412	0.7647412
	16	0.6066703	0.6067173	0.6067172	0.7647773	0.7647412	0.7647412
	40	0.6066703	0.6067173	0.6067172	0.7647773	0.7647412	0.7647412
100	4	0.6063824	0.6064106	0.6064105	0.7646507	0.7646145	0.7646145
	8	0.6064310	0.6064780	0.6064778	0.7646464	0.7646103	0.7646102
	16	0.6064309	0.6064778	0.6064778	0.7646464	0.7646103	0.7646102
	40	0.6064309	0.6064778	0.6064778	0.7646464	0.7646103	0.7646102

sessment should be made regarding the accuracy of the numerical evaluation of the spectral transmittance using Eq. (9). Since it is a multidimensional integral, a priori theoretical assessment of the error involved cannot be made. To achieve an accurate evaluation, the convolution integral must be divided into a large number of finite interval integrals, and each of these multidimensional integrals is evaluated using quadrature formulas. Since the ILS has the largest impact on the accuracy, the choice has been made to consider a large number of finite interval integrals, with each spanning a half-period of the oscillation. Over a half-period, the integrand varies smoothly.

Table 1 shows the convergence of the synthetic spectral transmittance at one wave number belonging to the P branch of CO and another to the ν_1 and ν_3 bands of H_2O. The synthetic partial-pressure profiles are given in Table 1, whereas the synthetic temperature profile is $\tilde{T} = 1300 - 800z^2$. Inspection of Table 1 reveals that the numerical evaluation of the integral along the LOS in Eq. (3) yields a transmittance that is accurate to seven digits using an eight-point quadrature (N_x). Since higher-order quadratures may be required for other temperature and partial-pressure profiles, a 16-point quadrature is used in this analysis.

Table 1 also shows that an eight-point quadrature over each half-period of the ILS (N_ν) leads to better than seven-digit accuracy. At the considered pressures, the HWHH of individual lines is on the order of 0.5 cm^{-1}, meaning that the true spectral transmittance will vary smoothly over each half-period for many spectral lines. As the pressure decreases or the temperature increases, the width of most lines (those with a positive temperature exponent) decreases according to Eq. (7). When this occurs, the spectral transmittance becomes a sharply peaked function, requiring a modification of numerical integration over each half-period to maintain the desired accuracy.

The number of finite interval integrals N_p used in the evaluation of Eq. (9) has the greatest effect on the numerical accuracy of the spectral transmittance. Figure 2 shows the synthetic spectrum calculated with $N_p = 100$, as well as the difference in synthetic spectrum computed by subtracting the spectral transmittance with $N_p = 50$ or 30 from the one calculated with $N_p = 100$. This difference represents the error in truncating the convolution integral. Examination of Fig. 2 reveals that at 2000 cm^{-1}, the difference is 0.0005 for $N_p = 30$ and 0.0003 for $N_p = 50$. Retaining too few finite interval integrals may lead to significant errors in the computed spectral transmittance. More importantly, errors resulting from truncating the convolution integral of Eq. (9) will maintain the shape of the true transmittance and will affect the deduced temperature and partial-pressure profiles. The use of 200 finite interval integrals, $N_p = 100$, should provide a four-digit accuracy, but it requires that the spectral transmittance be calculated 100 cm^{-1} beyond the spectral ranges of the input data.

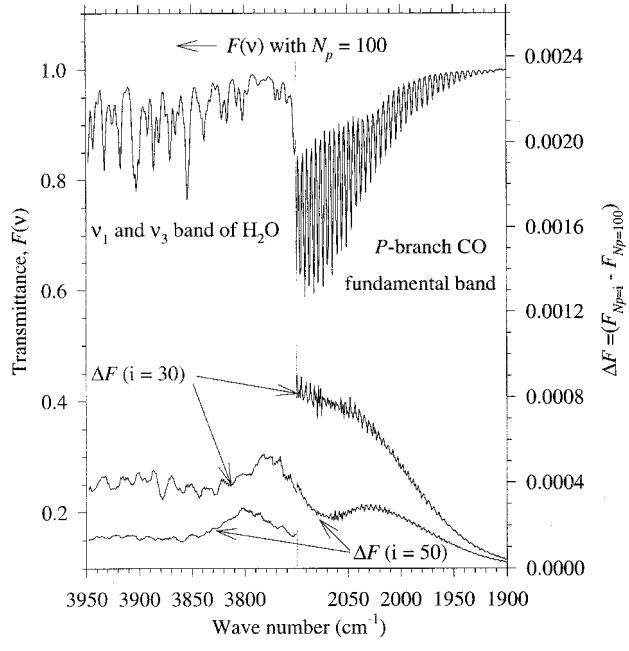

Fig. 2 Spectral transmittance computed using $N_p = 100$, as well as the difference of spectral transmittance computed by using $N_p = 30$ and 50.

Recovery of Temperature and Species Profiles

The two-step inverse procedure was tested for its robustness using six cases with synthetic values and the results shown in Table 2. For these six cases and the results shown in Figs. 3–6, both the synthetic and the modeled temperature and species profiles utilized a second-order approximation of the power series of Eqs. (10). An initial guess of 1 atm for the partial pressures of both CO and H_2O and a temperature of 600 K were used. All cases converged to within 1% of the true temperature and partial-pressure profiles. Case 6 showed the largest deviation of 0.7%, in the second-order coefficient ($\hat{P}^2_{H_2O,1}$) of H_2O. Step 1 converged within six iterations for all cases, showing only slight changes in the LOS average values past the third iteration. Step 2 converged in less than 14 iterations for all cases, except in case 6, which required over 30

Table 2 Coefficients for temperature and partial-pressures profiles used to generate synthetic data (input), as well as results of the inverse analysis (output)

	$T = T_0 + T_1 z^2$		$P_{CO} = P_{CO,0} + P_{CO,1} z^2$		$P_{H_2O} = P_{H_2O,0} + P_{H_2O,1} z^2$	
Case	T_0	T_1	$P_{CO,0}$	$P_{CO,1}$	$P_{H_2O,0}$	$P_{H_2O,1}$
1						
Input	1300	−800	2.5	−1.25	2.5	−1.25
Output	1300.00	−800.00	2.500	−1.2500	2.500	−1.250
2						
Input	1600	−800	2.5	−1.25	2.5	−1.25
Output	1600.01	−799.99	2.500	−1.250	2.500	−1.250
3						
Input	900	−500	2.5	−1.25	2.5	−1.25
Output	900.00	−499.89	2.500	−1.250	2.500	−1.250
4						
Input	1300	−800	1.25	1.25	2.5	−1.25
Output	1300.00	−800.00	1.250	1.250	2.5	−1.25
5						
Input	1300	−800	1.25	1.25	1.25	1.25
Output	1300.00	−800.00	1.250	1.250	1.25	1.25
6						
Input	1000	0	2.5	−1.25	2.5	−1.25
Output	1000.64	−2.284	2.500	−1.2522	2.509	−1.259

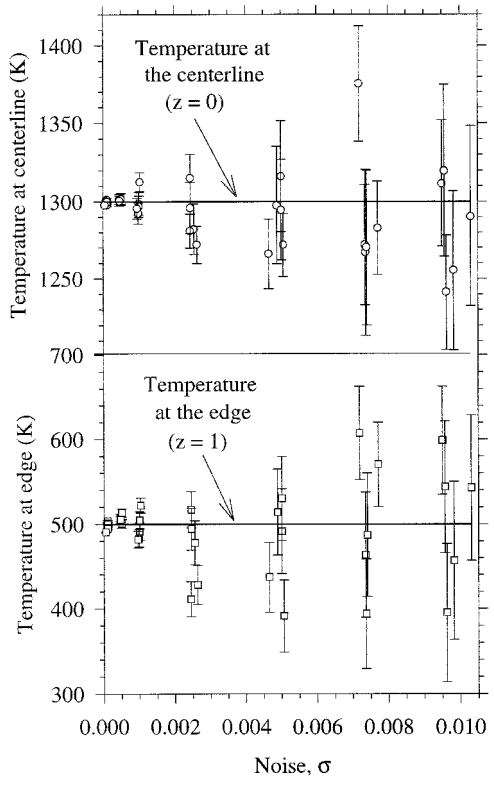

Fig. 3 Effect of noise on the temperature at the centerline and at the edge of the flame. Points represent the results from the inverse technique with a 65% confidence level as predicted from the diagonal terms of the covariant matrix.[23]

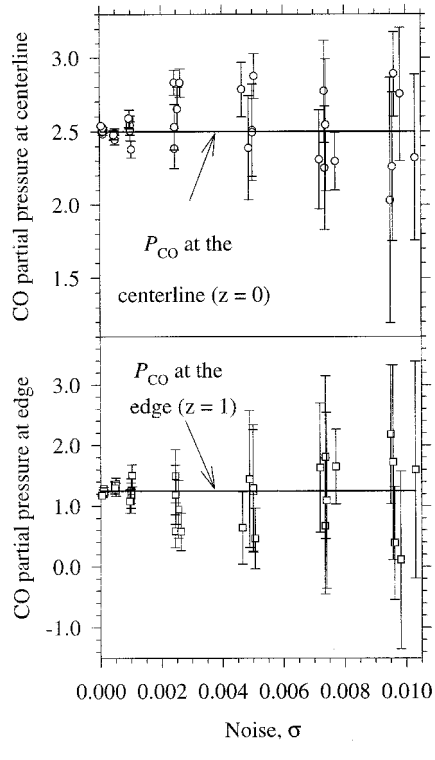

Fig. 4 Effect of noise on the partial pressure of CO at the centerline and at the edge of the flame. Points represent the results from the inverse technique with a 65% confidence level as predicted from the diagonal terms of the covariant matrix.[23]

iterations. Again, only minor changes in the temperature and species profiles were seen after the eighth or ninth iteration. During the first four or five iterations of step 2, significant improvements in the temperature profile occurred with only minor changes in the partial-pressure profiles. At this point in the inverse algorithm, the spectral dependence of the transmittance on temperature through Eq. (5) is controlling the convergence. After the temperature profile is sufficiently close to the synthetic one, the partial-pressure profiles rapidly converge toward their synthetic ones. This should be expected since the effect of the partial-pressure profile on the spectral transmittance is dependent on the temperature profile through the integration over the LOS in Eq. (3). Although the spectral transmittance shows some variations with partial pressures through the shape of individual lines in Eq. (7), this dependency is an order of magnitude smaller than the effects from Eqs. (3) and (5). Under certain circumstances, such as a constant temperature, the species dependency in Eq. (7) is very important for achieving the convergence of the inverse algorithm.

Case 6 is a difficult situation to solve because the temperature is constant along the LOS. In this case, the algorithm must rely on the species dependency in the line shape in Eq. (7) to guide the solution. The partial-pressures profiles of different species are highly coupled in the inverse analysis, since each gaseous species contributes to the line shape through the collisional broadening reference HWHH. The effect of temperature is also seen in Eq. (7), leading to a curvature matrix

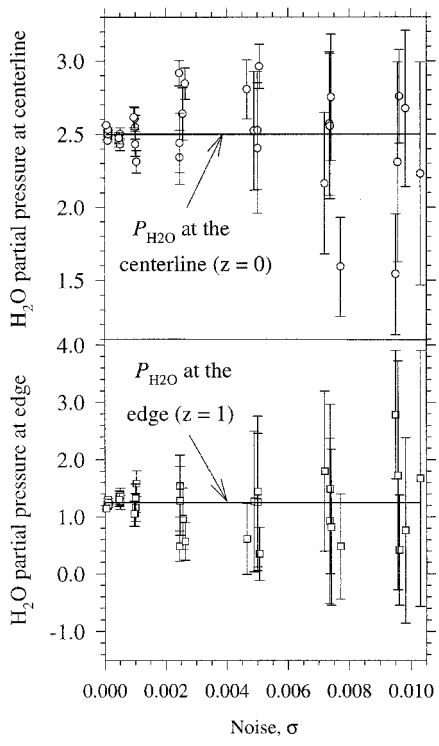

Fig. 5 Effect of noise on the partial pressure of H_2O at the centerline and the edge of the flame. Points represent the results from the inverse technique with a 65% confidence level as predicted from the diagonal terms of the covariant matrix.[23]

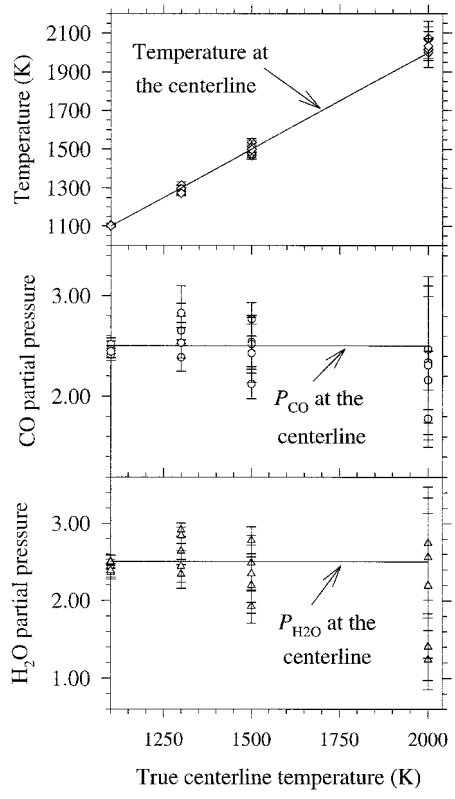

Fig. 6 Effect of centerline temperature on the estimated temperature and partial pressures of CO and H_2O at the center of the flame using $2L$ = 0.005 m and σ = 0.0025. Points represent the results from the inverse technique with a 65% confidence level as predicted from the diagonal terms of the covariant matrix.[23]

that is highly coupled in the six unknown coefficients. Hence, a large number of iterations was required to reach the converged solution.

Effect of Noise

The second portion of the results is focused on the influence of noise on the deduced temperature and partial-pressure profiles. Transmittance measurements through the flame of a burning nitramine-composite propellant using a Nicolet 740 spectrometer with a mercury cadmium telluride detector and potassium bromide beam splitter have been performed in our laboratory. A measured noise of 0.004, based on χ^2 statistics, was obtained by averaging four consecutive spectra. This is compared to a measured noise of 0.002, taken under similar conditions, when the flame is not present. The increased noise level within the flame can be attributed to the effects of particle ejection from the burning surface, intermittent and nonuniform burning, and purge-gas flow around the periphery of the flame. FTIR systems currently available may have an order of magnitude higher signal-to-noise than the 740 system, because of the advances in blackbody sources, detectors, and system optics. Measured noise using the Nicolet 740 system with and without a flame are well represented by a Gaussian distribution. Therefore, in this work, a Gaussian noise distribution was added directly to the synthetic spectral transmittances. Hence, the spectral transmittances containing random noise are computed from

$$\tilde{F}_{\text{noise}} = \tilde{F} + \omega\sigma \tag{12}$$

where the pseudorandom noise with a Gaussian distribution is generated using RAN1 and GASDEV subroutines from Ref. 21. Thirty-five new spectra were computed by adding random noise with $0.0001 \leq \sigma \leq 0.01$ to the spectral transmittances corresponding to case 1 of Table 2.

Variations caused by random noise in the recovered temperature and partial pressures of CO and H_2O at the center and edge of the simulated flame are given in Figs. 3–5, respectively. The LOS average temperature determined during step 1 is insensitive to the noise level and has a value of 998 ± 9 K (20:1). At the centerline, it is off by over 300 K. After step 2, Fig. 3 shows that the maximum deviation in the centerline temperature is 70 K, and that in most cases the centerline temperatures are within 50 K of the synthetic value. It is quite difficult to measure the temperature in a propellant flame to within this accuracy (50 K) using either intrusive or nonintrusive techniques. The temperature at the edge shows a slightly greater deviation from the synthetic value (maximum difference of 120 K), but values at the edge are not of strong interest. Confidence bounds calculated using only the diagonal terms of the covariant matrix[23] also predict this trend. The integration over the LOS tends to desensitize coefficients associated with higher-order terms of the polynomials describing the temperature and partial-pressure profiles.

Figure 4 shows that the partial pressure of CO at the centerline is within 20% of the actual partial pressures for all cases, whereas the LOS average value of 1.98 ± 0.02 (20:1) from step 1 is off by 25% at the centerline. Similar to the temperature, the partial pressure of CO at the edge shows a greater deviation than at the centerline. For H_2O in Fig. 5, there are a few cases that deviate significantly from the synthetic value at both the centerline and the edge, but most of the centerline partial pressures are within 20% of the synthetic value. The LOS average H_2O partial pressure is 2.03 ± 0.04 (20:1) atm. The H_2O band used in this analysis has a different spectral structure than CO; more specifically, this H_2O band shows a smaller variation in absorption coefficient with rotational index number. This leads to a smaller spectral dependence on temperature and partial pressures than in the CO ν_0 band, causing the algorithm to be less sensitive to the H_2O partial-pressure profile as the noise increases. A different choice of H_2O band for the analysis may help to improve the accuracy of the estimated partial-pressure profile of H_2O. How-

ever, it is likely that other bands of H_2O, such as the one centered at 1595 cm^{-1}, interfere with other important IR-active molecules, requiring the consideration of overlapping.

The temperature and species profiles are generally unaffected by noise levels below 0.001. As the noise increases much beyond 0.001, the temperature and partial-pressure profiles are more difficult to reproduce with an acceptable confidence. The deviation in spectral transmittance between using LOS average and LOS variations in temperature and partial pressures is on the order of 0.01. As the noise reaches this level, it becomes increasingly difficult to deduce accurate profiles, because the algorithm cannot distinguish between the changes that occur in the spectral transmittances caused by noise and those caused by spatially varying temperature and partial pressure. In general, the estimated partial-pressure profiles are more affected by noise than the temperature profile. This effect occurs as a result of error propagation from the estimated temperature profile into the estimated partial-pressure profiles through the coupling effect of the integration in Eq. (3). The actual cutoff limit caused by noise is dependent on the physical parameters of the system: path length, temperature, and total and partial pressures.

When examining the flame structure of a solid propellant using optical methods, it is important to understand the effect of noise as the temperature increases. Fine-wire thermocouple measurements taken during the combustion of a nitramine-composite propellant[2] indicate a large variation in temperature along the centerline. The thermocouple traces revealed a three-zone flame structure, with a temperature of about 1000 K near the surface and about 2000 K near the luminous flame. The effect of the synthetic centerline temperature on the recovered one, assuming constant noise, is explored to assess the ability of the inverse analysis to probe the flame structure of a nitramine-composite propellant.

Figure 6 shows the effect of the synthetic centerline temperature on the ability to recover the centerline temperature and partial pressures. The synthetic spectra were generated using the partial-pressures profiles of CO and H_2O from case 1 in Table 2. The centerline temperature varied from 1100 to 2000 K, with an 800 K difference between the centerline to the edge of the flame. Pseudorandom noise with an average deviation of 0.0025 was added to the synthetic spectral transmittance given by Eq. (12). As the temperature increases, it becomes increasingly more difficult to recover accurate values of centerline temperature and partial pressures. The redistribution in rotational and vibrational states with higher temperature tends to reduce the absorptance near the band center, while slightly increasing the absorptance in the wings of the rovibrational band. This results in a decrease in the effect of spatial variations in temperature and species mole fractions over the range of spectral transmittances. While this variation was on the order of 0.01 at 1300 K, it is on the order of 0.005 at 2000 K. Therefore, at 2000 K with an average noise of 0.0025, the inverse analysis experiences an increased difficulty in recovering accurate estimates in the centerline temperatures and species concentrations.

The inverse analysis is able to predict centerline temperatures within 100 K at this noise level (0.0025) for all temperature profiles considered. In every case, the deduced centerline temperature from step 2 showed an improvement over the LOS-average temperature found in step 1. Recovered centerline partial pressures are within 20% of their true value as long as the temperature remains below about 1500. Beyond this temperature limit, the inverse algorithm does not consistently show improvements in the recovered centerline partial pressures from step 1 to step 2. It should be noted that this temperature limit is affected by path length, noise level, total pressure, and species concentrations.

In an actual flame, the temperature and species profiles are unknown and may not be well represented by a second-order power series. The ability of the inverse technique to recover more realistic profiles by using higher-order power series approximations for temperature and partial-pressure profiles should therefore be assessed. A synthetic spectrum is generated using exponential functions for the profiles of both temperature [$\tilde{T} = 1331.64 - 31.64 \exp(3.269z^2)$] and partial pressures [$\tilde{P}_{CO} = \tilde{P}_{H_2O} = 2.5494 - 0.0494 \exp(3.269z^2)$]. Coefficients of a successively higher-order power series are determined from the synthetic transmittance spectrum.

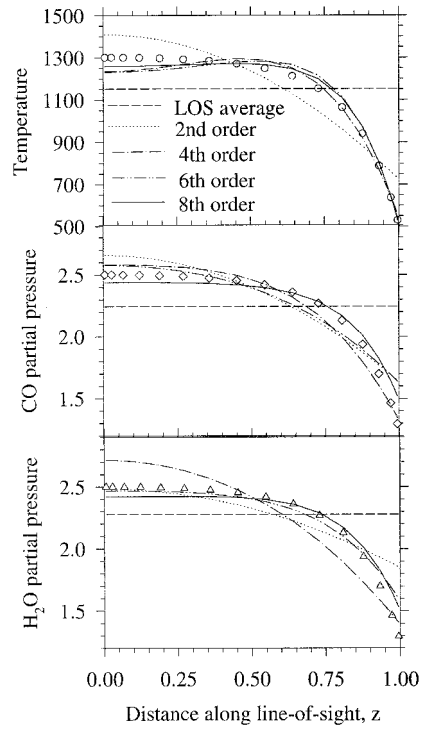

Fig. 7 Comparison of the temperature and the species (CO and H_2O) profiles determined from the inverse analysis using power series approximations to the input synthetic exponential profiles (symbols).

Figure 7 shows the ability to recover the synthetic exponential profiles for temperature and partial pressures by using the successively increased order of the power series representation given by Eq. (10). That is, the eighth-order case involves 15 unknown constants to be determined. The synthetic spectrum contains random noise with a standard deviation of 0.001. Within the figure, the open-faced symbols represent the input synthetic temperature and partial-pressure profiles, whereas the lines represent the recovered values. The LOS values found in step 1 considerably underpredict the synthetic centerline values. At this noise level, the inverse analysis shows only a marginal improvement in recovering the centerline values as well as the overall profiles beyond a sixth-order power series. Centerline temperature and partial pressures of CO and H_2O are within 5% of the synthetic centerline values for all profiles greater than sixth order.

Summary and Conclusions

The development of a nonlinear, least-squares-based inverse method for deducing temperature and partial-pressure profiles of CO and H_2O from spectral transmittance data is presented. The analysis utilizes synthetic spectral transmittances acquired by an FTIR spectrometer operating at a low spectral resolution and a single LOS. The analysis assumed that the temperature and species profiles can be represented by polynomials with coefficients that are to be determined, and it accounts for the effects of noise. Noise levels below 0.001 have little effect on the solution. Because changes in the spectral transmittances caused by noise are on the same level as those changes caused by spatial variations in temperature and species concentrations, the algorithm experiences difficulties in maintaining accuracy.

Temperature appears to be slightly less sensitive to noise than the partial pressures of CO and H_2O, with H_2O partial pressure being the most sensitive. Changing the flame temperature also affects the ability of the inverse algorithm to recover centerline temperature and partial pressures. As the temperature increases, changes in spectral transmittances caused by spatial variations of temperature and species concentrations decreases, thereby requiring an increased signal-to-noise ratio to recover accurate temperature and species concentrations. More realistic temperature and species profiles can be recovered by using higher-order power series approximations.

Future Work

In the future, additional IR-active molecules will be added to the data-reduction routine. The model can be easily implemented by other LOS techniques for temperature and species profiling, such as uv/visible and multichannel IR spectroscopy. The determination of collision broadening parameters for other molecules is also needed to extend this method to high-temperature gases containing other IR-active molecules, such as CO_2, N_2O, NO, HCN, and C_nH_m.

Acknowledgments

This work was performed under Contract DAAL03-92-G-0118 and supported by R. W. Shaw of the U.S. Army Research Office, Research Triangle Park, North Carolina.

References

[1]Parr, T., and Hanson-Parr, D., "Nonintrusive Diagnostic Techniques for Research on Nonsteady Burning of Solid Propellants," *Nonsteady Burning and Combustion Stability of Solid Propellants*, edited by L. De Luca, E. W. Price, and M. Summerfield, Vol. 143, Progress in Astronautics and Aeronautics, AIAA, Washington, DC, 1992, pp. 261–324.

[3]Lu, Y. C., Freyman, T. M., and Kuo, K. K., "Measurement of Temperatures and OH Concentrations of Solid Propellant Flames Using Absorption Spectroscopy," *Combustion Science and Technology*, Vol. 104, Nos. 1–3, 1995, pp. 193–205.

[3]Modiano, S. H., and Vanderhoff, J. A., "Multichannel Infrared Absorption Spectroscopy of Solid Propellant Flames," *Combustion and Flame*, Vol. 99, No. 1, 1994, pp. 187–189.

[4]Mallery, C. F., Kim, E. S., and Thynell, S. T., "High-Pressure Strand Burner System for Propellant Flame Studies Using Absorption Spectroscopy," *Review of Scientific Instruments*, Vol. 66, No. 8, 1995, pp. 4091–4094.

[5]Thorne, L. R., and Melius, C. F., "The Structure of Hydrogen Cyanide-Nitrogen Dioxide Premixed Flames," *23rd Symposium (International) on Combustion*, The Combustion Inst., Pittsburgh, PA, 1990, pp. 397–403.

[6]Huang, I. T., Thynell, S. T., and Kuo, K. K., "FT-IR Spectroscopy of Laminar Premixed Hydrocarbon/Air Flames," *3rd International Symposium on Non-Intrusive Combustion Diagnostics*, edited by K. K. Kuo and T. Parr, Begell House, Inc., New York, 1994, pp. 209–226.

[7]McNesby, K. L., Daniel, R. G., Morris, J. B., and Miziolek, A. W., "Tomographic Analysis of CO Absorption in a Low-Pressure Flame," *Applied Optics*, Vol. 34, No. 18, 1995, pp. 3318–3324.

[8]Best, P. E., Chen, P. L., Carangelo, R. M., Solomon, P. R., Danchak, M., and Ilovici, I., "Tomographic Reconstruction of FT-IR Emission and Transmission Spectra in a Sooting Laminar Diffusion Flame: Species Concentrations and Temperatures," *Combustion and Flame*, Vol. 85, No. 3/4, 1991, pp. 309–318.

[9]Cremers, C. J., and Birkebak, R. C., "Application of Abel's Integral Equation to Spectrographic Data," *Applied Optics*, Vol. 5, No. 6, 1966, pp. 1057–1064.

[10]Liau, Y.-C., and Yang, V., "Analysis of RDX Monopropellant Combustion with Two-Phase Subsurface Reactions," *Journal of Propulsion and Power*, Vol. 11, No. 4, 1995, pp. 729–739.

[11]Prasad, K., Yetter, R. A., and Smooke, M., "An Eigenvalue Approach for Computing the Burning Rate of RDX Propellants," AIAA Paper 96-2884, July 1996.

[12]Yetter, R. A., Dryer, F. L., Allen, T., and Gatto, J., "Analysis of Elementary Models for the Steady-State Combustion of Solid Propellants," *Journal of Propulsion and Power*, Vol. 11, No. 4, 1995, pp. 666–676.

[13]Melius, C. F., "Thermochemical Modeling: I & II," *Chemistry and Physics of Energetic Materials*, edited by S. N. Bulusu, Kluwer Academic, Norwell, MA, 1990, pp. 21–78.

[14]Griffiths, P. R., and De Haseth, J. A., *Fourier Transform Infrared Spectrometry*, Wiley, New York, 1986, Chaps. 1–3.

[15]Griffith, D. W. T., "Synthetic Calibration and Quantitative Analysis of Gas-Phase FT-IR Spectra," *Applied Spectroscopy*, Vol. 50, No. 1, 1995, pp. 59–70.

[16]Rothman, L. S., Gamache, R. R., Tipping, R. H., Rinsland, C. P., Smith, M. A. H., Benner, D. C., Devi, V. M., Flaud, J.-M., Camy-Peyret, C., Perrin, A., Goldman, A., Massie, S. T., Brown, L. R., and Toth, R. A., "The HITRAN Molecular Database: Editions of 1991 and 1992," *Journal of Quantitative Spectroscopy and Radiative Transfer*, Vol. 48, No. 5/6, 1992, pp. 469–507.

[17]Hartmann, J. M., Rosenmann, L., Perrin, M. Y., and Taine, J., "Accurate Calculated Tabulations of CO Line Broadening by H_2O, N_2, O_2 and CO_2 in the 200–3000K Temperature Range," *Applied Optics*, Vol. 27, No. 15, 1988, pp. 3063–3065.

[18]Nakazawa, T., and Tanaka, M., "Measurement of Intensities and Self- and Foreign-Gas-Broadened Half-Widths of Spectral Lines in the CO Fundamental Band," *Journal of Quantitative Spectroscopy and Radiative Transfer*, Vol. 28, No. 5, 1982, pp. 409–416.

[19]Delaye, C., Hartmann, J. M., and Taine, J., "Calculated Tabulation of H_2O Line Broadening by H_2O, N_2, O_2 and CO_2 at High Temperature," *Applied Optics*, Vol. 28, No. 23, 1989, pp. 5080–5087.

[20]Gamache, R. R., and Rothman, L. S., "Temperature Dependence of N_2-Broadened Halfwidths of Water Vapor: The Pure Rotation and ν_2 Bands," *Journal of Molecular Spectroscopy*, Vol. 128, No. 2, 1988, pp. 360–369.

[21]Press, W. H., Teukolsky, S. A., Vetterling, W. T., and Flannery, B. P., *Numerical Recipes*, Cambridge Univ. Press, Cambridge, MA, 1992, Chaps. 4, 7, and 15.

[22]Özisik, M. N., *Heat Conduction*, 2nd ed., Wiley, New York, 1993, Chap. 14.

[23]Ho, C.-H., and Özisik, M. N., "An Inverse Radiation Problem," *International Journal of Heat and Mass Transfer*, Vol. 32, No. 2, 1989, pp. 335–341.

[24]Fifer, R. A., "Chemistry of Nitrate Ester and Nitramine Propellants," *Fundamentals of Solid Propellant Combustion*, edited by K. K. Kuo and M. Summerfield, Vol. 90, Progress in Astronautics and Aeronautics, AIAA, New York, 1984, pp. 177–237.

[25]Ho, C.-H., and Özisik, M. N., "Inverse Radiation Problems in Inhomogeneous Media," *Journal of Quantitative Spectroscopy and Radiative Transfer*, Vol. 40, No. 5, 1992, pp. 553–560.